Chemical Physics 370 (2010) 87–97

Contents lists available at ScienceDirect

Chemical Physics

journal homepage: www.elsevier.com/locate/chemphys

Linearized approximations for condensed phase non-adiabatic dynamics: Multi-layered baths and Brownian dynamics implementation

P. Huo [a], S. Bonella [c], L. Chen [d], D.F. Coker [a,b,*]

[a] Department of Chemistry, Boston University, 590 Commonwealth Avenue, Boston, MA 02215, United States
[b] Department of Physics, University College Dublin, Belfield, Dublin 4, Ireland
[c] Dipartimento di Fisica, Università "La Sapienza", Piazzale Aldo Moro, 2, 00185 Roma, Italy
[d] Department of Chemistry, University of Illinois, Urbana-Champagne, 505 South Mathews Avenue, Urbana, IL 61801, United States

ARTICLE INFO

Article history:
Received 20 October 2009
In final form 21 February 2010
Available online 25 February 2010

Keywords:
Non-adiabatic
Linearized approximation
Hierarchical bath
System-bath
Open system
Quantum dynamics
Influence functional
Brownian oscillator

ABSTRACT

Several approximate methods for propagating the density matrix of systems coupled to baths based on linearized approximations have been presented. Using influence functional formalism this approximation is explored in various limits for a condensed phase model. A new iterative stochastic propagation scheme is introduced that integrates out some of the bath degrees of freedom giving an effective evolution resembling Brownian dynamics. We show that this approach satisfies the fluctuation–dissipation theorem in various limits. The method is compared with alternative approximate full dimensional propagation schemes for the spin-boson model. The accuracy of the results is surprising since the scheme makes approximations about initialization at each iteration. This accuracy is encouraging since these kind of approaches hold significant potential computational saving for condensed phase quantum dynamics simulations as they give a systematic way of eliminating the explicit integration of a large number of environmental degrees of freedom.

1. Introduction

Recent work in the field of mixed quantum-classical dynamics [1–8] has employed linearized approximations to the evolution of the full system. The linearized approximation is applied in particular when calculating the time dependent density matrix of a non-equilibrium system or equilibrium time correlation functions. The general idea is to first separate the interacting degrees of freedom of the condensed phase system of interest into a quantum subset and a classical bath based on relative thermal wavelength or energy considerations. The forward and backward time propagators in the evolution of the density matrix, or of the correlation function, are represented as path integrals. The phase in the integrands of these expressions is then expanded to linear order in the difference between the forward and backward paths of the bath. The resulting approximate form still contains the full evolution of the quantum subsystem. If an appropriate representation for this dynamics is available (e.g. the mapping Hamiltonian or some semiclassical formulation) the linearized approximation can be computed using classical trajectories. While the benefits of the truncation to linear order in the difference paths for the bath variables are well known and have been exploited in a number of applications [9–13], work is still in progress to obtain a general understanding of the conditions under which the approximation is reliable [14].

Depending on the interplay between the parameters in the Hamiltonian, the linearized expression can provide a good approximation for evolving the density matrix over different periods of time. When the linearized approximation is reliable only for short times, correction schemes can be applied. Recently, an iterative scheme employing the linearized approximation for the mixed quantum-classical propagator in the mapping Hamiltonian formulation as a short time approximation in a path integral expression for long time propagation has been suggested [15]. The approach provides a systematic way to extend the linearized approximation to longer times but this comes at a numerical cost that can be substantially reduced in conditions where linearization is reliable for longer times. Similar computational problems affect the work of other groups that have proposed employing approximate short time propagators to iteratively evolve the density matrix. For example, Kapral, Ciccotti, and co-workers have developed an iterative solution for the mixed quantum-classical Wigner-Liouville equation [16–18] based on the Dyson series. The term that is lowest order in the interaction between the quantum and classical subsystems in the propagator gives the classical Liouvillian. Higher

* Corresponding author. Address: Department of Chemistry, Boston University, 590 Commonwealth Avenue, Boston, MA 02215, United States. Tel.: +1 617 353 2490; fax: +1 617 353 6466.
E-mail address: coker@bu.edu (D.F. Coker).

0301-0104/$ - see front matter © 2010 Elsevier B.V. All rights reserved.
doi:10.1016/j.chemphys.2010.02.021

order terms are represented as combinations of classical dynamics and transitions among states.

Given the computational advantages of the fully linearized scheme, an appreciation of how it becomes accurate for model systems important in condensed phase chemical physics is crucial. In this work we consider and explore one such model: a quantum system is coupled to a local bath, which in turn interacts with an environment represented as a set of harmonic oscillators with bilinear coupling. Such multi-level baths have been studied in various contexts from the early work of Garg et al. [19], who used a very similar path integral influence functional approach to the one we employ here, to explore the qualitative effects of environmental friction and solvent modes (the global bath) on the nuclear reaction coordinates (the local bath) in determining, for example, electron transfer rates (the quantum subsystem). The various approaches we develop here, however, offer a general methodology for developing mixed quantum-classical trajectory based methods, built on these ideas, to propagate an approximation to the density operator for such systems. The same basic ideas underlie the Brownian oscillator models [20,21] that have been so pivotal in the development of the theory of nonlinear spectroscopy of complex systems. More recently [22,23], the spin-boson model with a hierarchical, Brownian oscillator-like bath was employed to develop an approach that combines accurate quantum dynamics for the local bath together with a master equation for the global bath. This marriage of different quantum dynamics methodologies to treat different parts of a system is the powerful idea that forms the basis of the methods we develop in this paper.

A similar model, employing only one harmonic local bath mode, has been used by Shiokawa and Kapral [24] to study the emergence of quantum-classical dynamics in an open quantum environment. These authors showed how the relative time-scales of the quantum subsystem and local bath coherent dynamics change depending on the couplings and on the choice of the model for the spectral density (Ohmic and super-Ohmic) for the baths. In particular, they found that, at high temperatures and for weak couplings, the onset of decoherence can be much faster for the local bath than for the quantum subsystem thus enabling a mixed quantum-classical description of the combined system. This analysis was based on the influence functional formalism [25], which has a long history of development and application, starting in the context of open system dynamics with the early work of Caldeira and Leggett and others [26,27] who investigated the dissipative dynamics of a quantum system coupled to a harmonic bath. In simulations, the influence functional approach has also been used by Makri and co-workers to study the reduced (quantum or semiclassical) dynamics of such systems [28]. As an alternative Pollak and coworkers have extended semiclassical initial value ideas and developed continuum limit methods for treating the quantum dynamics of open dissipative systems [29–31]. Shi and Geva [32], on the other hand, employed a path integral formalism to show how the mixed quantum-classical Liouville equation can be obtained, for given choices of the quantum subsystem basis (diabatic and adiabatic), from linearization of an influence functional. In all these numerical applications, the quantum subsystem was directly coupled to the harmonic bath. In this work we rely on the influence functional formalism to identify conditions in which our linearized dynamics is accurate for the hierarchical bath model outlined above. In the theory section we summarize the most relevant aspects-some known from the literature [27], some based on our developments of the influence functional approach and explore the characteristics of the dynamics of the system when an Ohmic spectral density is used for the local and global baths. As expected from the previous work [24], we find that the critical parameters that control the accuracy of the linearized dynamics for this system are the temperature, the cutoff frequencies of the bath's spectra, and the relative strength of the coupling among the various subsystems.

In addition to this analysis we present a new algorithm to efficiently simulate the evolution of this type of hierarchical bath model. The scheme takes advantage of the influence functional to integrate out the degrees of freedom of the global, harmonic, environment. The evolution of the quantum subsystem and of the local bath is thus reduced to a scheme that has similarities to Brownian dynamics. We show that this new approach satisfies the fluctuation–dissipation theorem in appropriate limits. The new algorithm is potentially very useful for reducing the numerical effort needed to compute the properties of condensed phase systems for which the hierarchical bath model is reasonable. The accuracy of the new algorithm will be tested in benchmark calculations exploring the relevant range of parameters in the special case of a spin coupled to a local harmonic bath (spin-boson), that is bilinearly coupled to a global harmonic environment.

2. Theory

2.1. Hierarchical system-bath model: an influence functional analysis

2.1.1. The model

Condensed phase chemical systems can often be represented in terms of a quantum system (e.g. electrons, protons, or high frequency vibrations, etc.) that may be influenced by its local environment, the "local bath". This local bath essentially screens the quantum subsystem from the rest of the environment or "global bath". For simplicity we will thus assume that there is no direct interaction between the quantum subsystem and the global bath, but the local environment and the quantum subsystem are coupled. The local and global baths also of course can interact in our model.

For convenience we will define the system-local bath interaction Hamiltonian

$$\hat{h}(\hat{s},\hat{r}) = \widehat{H}_s + V_b(\hat{r}) + \Phi_{s-b}(\hat{s},\hat{r}) \tag{1}$$

where $\widehat{H}_s$ is the quantum subsystem Hamiltonian, including the kinetic energy operator, $\hat{s}$ and $\hat{r}$ are the system and local bath coordinate operators respectively, and the full Hamiltonian for the condensed phase models we will consider is thus

$$\widehat{H} = \frac{\hat{p}^2}{2M_b} + \hat{h}(\hat{s},\hat{r}) + \sum_J \left[\frac{\widehat{P}_J^2}{2M_B} + \frac{1}{2}M_B\Omega_J^2\widehat{R}_J^2 + C_J\widehat{R}_J\hat{r}\right] \tag{2}$$

Here the last square bracketed term on the right hand side represents the global bath with phase space operators $\{P_J, R_J\}$ as a set of harmonic oscillators that are bilinearly coupled to the local bath coordinate operators $\hat{r}$, which, in principle, could be highly dimensional. While the Hamiltonian above is a well defined model when the values of the parameters C_J are small, it is known [27,24] that it can exhibit pathological behavior in the limit of strong coupling between the local and global bath. This behavior is usually corrected by modifying the Hamiltonian via the introduction of the so-called "counter-term", thus

$$\begin{aligned}\widehat{H}_{ct} &= \frac{\hat{p}^2}{2M_b} + \hat{h}(\hat{s},\hat{r}) + \sum_J \left[\frac{1}{2}\left(\frac{\widehat{P}_J^2}{M_B} + M_B\Omega_J^2\widehat{R}_J^2\right) + C_J\widehat{R}_J\hat{r} + \frac{C_J^2}{2M_B\Omega_J^2}\hat{r}^2\right] \\ &= \frac{\hat{p}^2}{2M_b} + \hat{h}(\hat{s},\hat{r}) + \sum_J \left[\frac{\widehat{P}_J^2}{2M_B} + \frac{1}{2}M_B\Omega_J^2\left(\widehat{R}_J + \frac{C_J}{M_B\Omega_J^2}\hat{r}\right)^2\right]\end{aligned} \tag{3}$$

The counter-term completes the square in the bilinear coupling between the baths and makes the hessian in the bath degrees of freedom positive definite for this model. The motion of all degrees of freedom is thus bound and this ensures that the coupling be-

tween the baths does not change the nature of the local bath-quantum subsystem problem. In the following, we describe our developments for the case of the simpler Hamiltonian Eq. (1) for notational convenience. The introduction of the counter-term, an additive term that depends only on the local bath coordinates, does not modify these developments since the necessary algebra is made possible by the structure of the Hamiltonian in the global bath variables. To stress this fact, we shall point out after the appropriate steps the, trivial, changes in the equations due to the possible presence of the counter-term. In the Results section, on the other hand, we shall perform calculations for both models to illustrate the onset of the pathological behavior and show how the introduction of the counter-term corrects it.

We represent the quantum subsystem in terms of a basis set of diabatic states, $|n\rangle$. The local and global baths are described in the coordinate basis, and the composite system states are tensor products $|r,R,n\rangle$, where r and R are, in principle, vectors of local and global bath variables respectively.

Time dependent properties of the system can be obtained from the density operator $\hat{\rho}(t)$, with matrix elements

$$\langle r,R,n|\hat{\rho}(t)|r',R',m\rangle = \langle r,R,n|e^{-i\widehat{H}t/\hbar}\hat{\rho}(0)e^{i\widehat{H}t/\hbar}|r',R',m\rangle \tag{4}$$

Suppose the initial density operator has the product form: $\hat{\rho}(0)=\hat{\rho}_s\hat{\rho}_b\hat{\rho}_B$. There has been considerable theoretical work aimed at understanding the ramifications of these types of initial conditions [33]. Exactly how to realize the factored bath initial condition in general is non-trivial. For our purposes we will suppose that the local bath variables are strongly coupled to the quantum subsystem but initially are only weakly coupled to the global environment making the factored bath initial condition reasonable (e.g. a few molecular vibrational degrees of freedom that are strongly coupled to an electronic transition but that are only weakly coupled to a solvent environment). For the purpose of exploration we can initialize the system any way we like and the factored initial condition is theoretically convenient [26,24,27]. In the following we shall focus on non-equilibrium experiments for which the quantum subsystem is initially prepared in some non-thermal mixture of states $|\psi^0\rangle$ by, for example, interaction with a fast laser pulse. We will thus be interested in the evolution of the initial quantum subsystem density matrix $\hat{\rho}_s(0)=|\psi^0\rangle\langle\psi^0|=\sum_{n^0}\sum_{m^0}c^*_{m^0}c_{n^0}|n^0\rangle\langle m^0|$, where the c_{n^0} are the amplitudes of the different basis states comprising the initial quantum subsystem state $|\psi^0\rangle$. We shall consider experiments that probe the quantum subsystem states. The quantity of interest is thus the reduced density matrix, whose elements are obtained from the full density by tracing over all the bath degrees of freedom

$$\begin{aligned}\rho^{red}_{nm}(t) &= \int dr^N \int dR^N \langle r^N,R^N,n|\hat{\rho}(t)|r^N,R^N,m\rangle \\ &= \int dr^N \int dR^N \int dr^0 \int dR^0 \int d\tilde{r}^0 \int d\widetilde{R}^0 \sum_{n^0}\sum_{m^0} c^*_{m^0}c_{n^0} \\ &\quad\times \langle r^N,R^N,n|e^{-i\widehat{H}t/\hbar}|r^0,R^0,n^0\rangle\langle r^0,R^0|\hat{\rho}_{b0}\hat{\rho}_{B0}|\tilde{r}^0,\widetilde{R}^0\rangle \\ &\quad\times \langle \tilde{r}^0,\widetilde{R}^0,m^0|e^{i\widehat{H}t/\hbar}|r^N,R^N,m\rangle \\ &= \sum_{n^0}\sum_{m^0} c^*_{m^0}c_{n^0}(\rho^{red}_{nm})^{n^0m^0}(t)\end{aligned} \tag{5}$$

Let us focus on just one of the contributing terms $(\rho^{red}_{nm})^{n^0m^0}(t)$.

The path integral representation of the forward propagator matrix elements in the above expression is

$$\begin{aligned}\langle r^N,R^N,n|e^{-i\widehat{H}t/\hbar}|r^0,R^0,n^0\rangle = &\int_{r(0)=r^0}^{r(t)=r^N}\mathscr{D}[r(t)]\int_{R(0)=R^0}^{R(t)=R^N} \\ &\times\mathscr{D}[R(t)]e^{\frac{i}{\hbar}S^0[r(t),R(t)]}T_{nn^0}[r(t)]\end{aligned} \tag{6}$$

with a similar result for the backward propagator. The environmental action along the forward path, for example, is

$$\begin{aligned}S^0[r(t),R(t)] &= S[r(t)]+\sigma[r(t),R(t)] \\ &= \int_0^t dt'\frac{1}{2}M_b\dot{r}^2(t')+\int_0^t dt'\sum_J\left\{\frac{1}{2}M_B\dot{R}_J^2(t')\right. \\ &\quad\left.-\left[\frac{1}{2}M_B\Omega_J^2R_J^2(t')+C_JR_J(t')r(t')\right]\right\}\end{aligned} \tag{7}$$

and the forward transition amplitude is

$$T_{nn^0}[r(t)] = \langle n|e^{-\frac{i}{\hbar}\hat{h}(r^{N-1})\epsilon}\cdots e^{-\frac{i}{\hbar}\hat{h}(r^0)\epsilon}|n^0\rangle \tag{8}$$

Note that, in the case of the Hamiltonian that includes the counter-term, Eq. (3), the only change in the equations above is that the definition of the function $S[r(t)]$ must be modified to include the quadratic term in the local bath potential, i.e. $S_{ct}[r(t)]=\int_0^t dt'[\frac{1}{2}M_b\dot{r}^2(t')-\sum_J\frac{C_J^2}{2M_B\Omega_J^2}r^2(t')]$. Using the results in Eqs. (7) and (8), the matrix element becomes

$$\begin{aligned}(\rho^{red}_{nm})^{n^0m^0}(t) = &\int dr^N\int dr^0\int d\tilde{r}^0\langle r^0|\hat{\rho}_b|\tilde{r}^0\rangle\int_{r(0)=r^0}^{r(t)=r^N}\mathscr{D}[r(t)] \\ &\times\int_{\tilde{r}(0)=\tilde{r}^0}^{\tilde{r}(t)=r^N}\mathscr{D}[\tilde{r}(t)]e^{\frac{i}{\hbar}(S[r(t)]-S[\tilde{r}(t)])}T_{nn^0}[r(t)]T^*_{mm^0}[\tilde{r}(t)]F[r(t),\tilde{r}(t)]\end{aligned} \tag{9}$$

where $F[r(t),\tilde{r}(t)]$ is the influence functional [25,34] that contains all the information concerning the global bath

$$\begin{aligned}F[r(t),\tilde{r}(t)] = &\int dR^N\int dR^0\int d\widetilde{R}^0\int_{R(0)=R^0}^{R(t)=R^N}\mathscr{D}[R(t)] \\ &\times\int_{\widetilde{R}(0)=\widetilde{R}^N}^{\widetilde{R}(t)=\widetilde{R}^0}\mathscr{D}[\widetilde{R}(t)] \\ &\times\langle R^0|\hat{\rho}_B|\widetilde{R}^0\rangle e^{\frac{i}{\hbar}(\sigma[r(t),R(t)]-\sigma[\tilde{r}(t),\widetilde{R}(t)])}\end{aligned} \tag{10}$$

Here, due to our chosen partitioning of the system, this influence functional is independent of quantum subsystem state, but this is not in general required [35].

2.1.2. The Caldeira–Leggett influence functional approach

Assuming that the global bath oscillators are initially in thermal equilibrium Feynman and Vernon [25] gave the following, well known, analytic expression for the influence functional:

$$\begin{aligned}F[r(t),\tilde{r}(t)] &= \exp\left[-\frac{1}{\hbar}\int_0^t dt'\int_0^{t'}ds'[r(t')-\tilde{r}(t')]\alpha_R(t'-s')[r(s')-\tilde{r}(s')]\right] \\ &\quad\times\exp\left[-\frac{i}{\hbar}\int_0^t dt'\int_0^{t'}ds'[r(t')-\tilde{r}(t')]\alpha_I(t'-s')[r(s')+\tilde{r}(s')]\right] \\ &= \exp\left(-\frac{1}{\hbar}\psi[r(t),\tilde{r}(t)]\right)\exp\left(-\frac{i}{\hbar}\phi[r(t),\tilde{r}(t)]\right)\end{aligned} \tag{11}$$

The kernels $\alpha_R(t'-s')$ and $\alpha_I(t'-s')$ specify the temporal nonlocality of the local bath variables that results from coupling to the global bath. There is a rich literature exploring approximations to the influence functional that involve localizing the integrands in time. Much of this work is described in reference [27]. In the following we will detail one specific way to localize the integrands that takes advantage of the explicit form of the kernels. These can be written in terms of the local bath-global bath spectral density

$$J(\Omega)=\frac{\pi}{2}\sum_J\frac{C_J^2}{M_B\Omega_J}\delta(\Omega-\Omega_J) \tag{12}$$

and are given by

$$\alpha_R(t'-s') = \frac{1}{\pi}\int_0^\infty d\Omega J(\Omega)\coth(\beta\hbar\Omega/2)\cos\Omega(t'-s') \tag{13}$$

and

$$\alpha_I(t'-s') = -\frac{1}{\pi}\int_0^\infty d\Omega J(\Omega)\sin\Omega(t'-s') \tag{14}$$

With the model cutoff Ohmic spectral density

$$\begin{aligned} J(\Omega) &= \eta\Omega, \quad \text{if } \Omega \leqslant \Omega_c \\ &= 0, \quad \text{if } \Omega > \Omega_c \end{aligned} \tag{15}$$

or the exponentially truncated version

$$J(\Omega) = \eta\Omega\exp[-\Omega/\Omega_c], \tag{16}$$

for example, the coupling constants have the following frequency dependence

$$C^2(\Omega) = \frac{2}{\pi}M_B\eta\Omega^2$$

and the frequencies are sampled from the uniform or exponential distributions, respectively [28]. The developments outlined below employ the exponentially truncated Ohmic spectral density.

Making the simplifying approximation that

$$\begin{aligned} \eta\Omega\coth(\beta\hbar\Omega/2) &= \frac{2\eta}{\beta\hbar}, \quad \text{if } \Omega \leqslant \frac{2}{\beta\hbar} \\ &= \eta\Omega, \quad \text{if } \Omega > \frac{2}{\beta\hbar} \end{aligned} \tag{17}$$

we readily obtain the following approximate expression for $\alpha_R(t'-s')$

$$\begin{aligned} \frac{\pi\alpha_R(\tau)}{\eta\Omega_c^2} \sim \frac{1}{[1+(\Omega_c\tau)^2]}\Bigg[\frac{2}{\beta\hbar\Omega_c} + \frac{e^{-\left(\frac{2}{\beta\hbar\Omega_c}\right)}}{[1+(\Omega_c\tau)^2]} \\ \times\left\{[1-(\Omega_c\tau)^2]\cos\left(\frac{2\tau}{\beta\hbar}\right) - 2\Omega_c\tau\sin\left(\frac{2\tau}{\beta\hbar}\right)\right\}\Bigg] \end{aligned} \tag{18}$$

for this situation. Here we have made use of the following integral and its derivatives with respect to various parameters

$$\int dx e^{-ax}\cos bx = \frac{e^{-ax}}{[a^2+b^2]}[b\sin bx - a\cos bx], \ \text{Re } a > 0 \tag{19}$$

We can proceed in a similar fashion [26] to evaluate the integrals in the phase factor in Eq. (11). Writing

$$\phi[r(t),\tilde{r}(t)] = \int_0^t dt'\int_0^{t'} ds'[r(t')-\tilde{r}(t')]\alpha_I(t'-s')[r(s')+\tilde{r}(s')], \tag{20}$$

recognizing that with the exponentially truncated Ohmic spectral density

$$\alpha_I(\tau) = \frac{\eta}{\pi}\frac{d}{d\tau}\int_0^\infty d\Omega e^{-\Omega/\Omega_c}\cos\Omega\tau = \frac{\eta}{\pi}\frac{dL}{d\tau}, \tag{21}$$

where

$$L(\tau) = \int_0^\infty d\Omega e^{-\Omega/\Omega_c}\cos\Omega\tau = \frac{\Omega_c}{1+(\Omega_c\tau)^2} \tag{22}$$

and changing variables to $\tau = (t'-s')$ and t', we have

$$\phi[r(t),\tilde{r}(t)] = \frac{\eta}{\pi}\int_0^t dt'[r(t')-\tilde{r}(t')]\int_0^{t'} d\tau[r(t'-\tau)+\tilde{r}(t'-\tau)]\frac{dL}{d\tau}(\tau) \tag{23}$$

Evaluating the τ integral by parts gives

$$\begin{aligned} \phi[r(t),\tilde{r}(t)] = \frac{\eta}{\pi}\Bigg\{[r(0)+\tilde{r}(0)]\int_0^t dt'L(t')[r(t')-\tilde{r}(t')] \\ -\Omega_c\int_0^t dt'[r^2(t')-\tilde{r}^2(t')] + \int_0^t dt'[r(t')-\tilde{r}(t')] \\ \times\int_0^{t'} d\tau L(\tau)[\dot{r}(t'-\tau)+\dot{\tilde{r}}(t'-\tau)]\Bigg\} \end{aligned} \tag{24}$$

where $\dot{r}$ indicates the derivative of r with respect to its argument.

We proceed by defining mean $\bar{r}(t) = [r(t)+\tilde{r}(t)]/2$ and difference $z(t) = [r(t)-\tilde{r}(t)]$ paths and simplify the above expression to obtain

$$\phi[\bar{r}(t),z(t)] = \frac{2\eta}{\pi}\int_0^t dt'[\bar{r}(0)L(t') - \Omega_c\bar{r}(t') + l(t')\dot{\bar{r}}(t')]z(t') \tag{25}$$

where we have assumed that the properties of the local bath-global bath coupling are such that the spectral density is characterized by a cutoff frequency, Ω_c, that is sufficiently large so that the lorentzian function $L(\tau)$, which is strongly peaked around $\tau = 0$, decays rapidly from its peak value compared to the slowly varying mean velocity, $\dot{\bar{r}}(t'-\tau) = [\dot{r}(t'-\tau)+\dot{\tilde{r}}(t'-\tau)]/2$, at various points along the paths [27]. If these conditions are satisfied we can replace the variation of any such slowly varying function that appears under an integral with the fast decaying lorentzian by its value at $\tau = 0$, and pull it out of the integral. This is how we evaluated the τ integration in the above enabling us to define $l(t') = \int_0^{t'} d\tau L(\tau)$. We find that $\lim_{t'\to\infty} l(t') = \pi/2$.

We can proceed in a similar fashion to simplify the real exponential amplitude modulation term in Eq. (11) controlled by the kernel $\alpha_R(\tau)$. We can write this exponent in terms of the difference path, $z(t')$, using the same transformations outlined above as

$$\begin{aligned} \psi[\bar{r}(t),z(t)] &= \int_0^t dt'\int_0^{t'} ds' z(t')\alpha_R(t'-s')z(s') \\ &= \int_0^t dt' z(t')\int_0^{t'} d\tau z(t'-\tau)\alpha_R(\tau) \end{aligned} \tag{26}$$

The approximate form of $\alpha_R(\tau)$ in Eq. (18), while not as simply behaved as the lorentzian function used in the above manipulations, is still a rapidly decaying function of time over a range of parameters, in particular in the large Ω_c limit as demonstrated in Fig. 1. Thus, assuming that $z(t'-\tau)$ is a slowly varying function of τ compared with the kernel $\alpha_R(\tau)$, we again evaluate the integral over τ by approximating the path difference function with its value at the maximum of α_R (i.e. for $\tau = 0$). The path difference function then becomes independent of τ and can be pulled out of the integral giving

$$\psi[\bar{r}(t),z(t)] \sim \int_0^t dt' z^2(t')\alpha(t') \tag{27}$$

where $\alpha(t') = \int_0^{t'} d\tau\alpha_R(\tau)$.

Recall that α_R is a parametric function of β,η, and Ω_c, (see Eq. (18)) so $\alpha(t')$, is also dependent on these parameters.

2.1.3. A discrete path integral form, and the multi-state mapping Hamiltonian representation

With the above simplifications, the influence functional takes the form $F[\bar{r}(t),z(t)] = e^{-\Phi_{IF}}$, where $\Phi_{IF} = (\psi+i\phi)/\hbar$. This result will be used in Eq. (9) but, to set the stage for the linearization approximation that we will perform below, two more preliminary steps are necessary. First, we express the path integral for the local bath in discrete form, dividing the total time into N steps of duration $\epsilon = t/N$. Second, we use the mapping Hamiltonian formulation

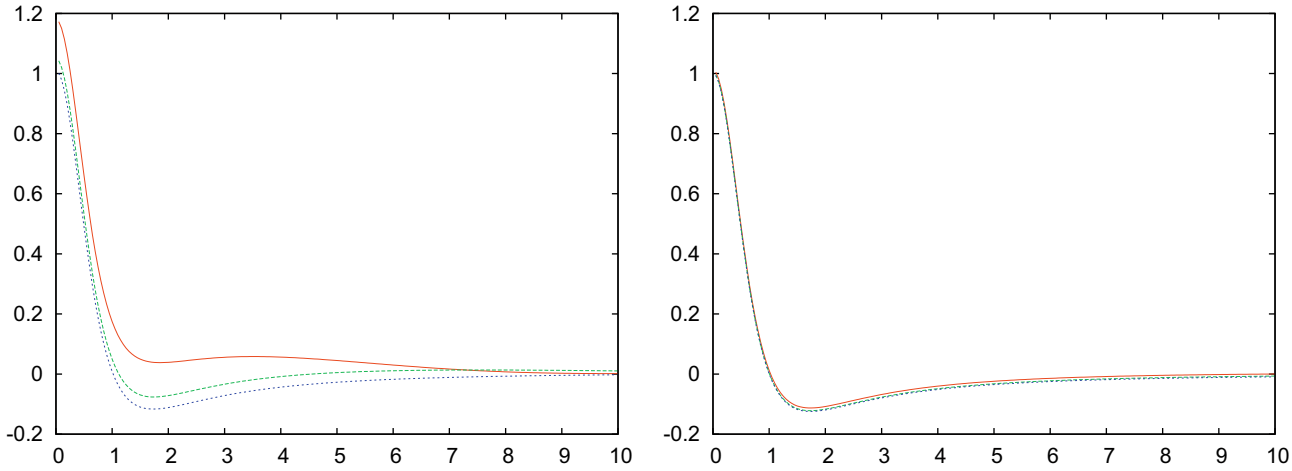

Fig. 1. Plots of $\pi\alpha_R/\eta\Omega_c^2$ as functions of $\Omega_c\tau$. Left panel has $\beta = 3$, right panel has $\beta = 12.5$, red curve is $\Omega_c = 1$, green curve is $\Omega_c = 2$, blue curve is $\Omega_c = 5$. (For interpretation of the references to colour in this figure legend, the reader is referred to the web version of this article.)

[36–39] to give a convenient, exact, representation of the transition amplitude, $T_{nn^0}(\{r_k\})$. A detailed description of these two steps can be found in Bonella and Coker [6], here we use the results derived in that reference to write

$$\begin{aligned}(\rho_{nm}^{red})^{n^0m^0}(t) = &\int dr^N \int dr^0 \int d\tilde{r}^0 \langle r^0|\hat{\rho}_b|\tilde{r}^0\rangle \delta(r_N - r^N)\delta(\tilde{r}_N - r^N)\\ &\times \int \prod_{k=1}^{N} dr_k \frac{dp_k}{2\pi\hbar} \prod_{k=1}^{N} d\tilde{r}_k \frac{d\tilde{p}_k}{2\pi\hbar} e^{i[S(\{r_k\})-S(\{\tilde{r}_k\})]}\\ &\times \int dp_q^0 dq^0 \int d\tilde{p}_q^0 d\tilde{q}^0 a_{n,t}(\{r_k\}) e^{i\Theta_{n,t}(\{r_k\})} a_{n^0,0} e^{-i\Theta_{n^0,0}} G_0\\ &\times \tilde{a}_{m,t}(\{\tilde{r}_k\}) e^{-i\tilde{\Theta}_{m,t}(\{\tilde{r}_k\})} \tilde{a}_{m^0,0} e^{i\tilde{\Theta}_{m^0,0}} \widetilde{G}_0 F[\{r_k\},\{\tilde{r}_k\}] \end{aligned} \quad (28)$$

In the expression above, and in the following, we set $\hbar = 1$. The expression for the transition amplitude

$$T_{nn^0}(\{r_k\}) = \int dp_q^0 dq^0 a_{n,t}(\{r_k\}) e^{i\Theta_{n,t}(\{r_k\})} a_{n^0,0} e^{-i\Theta_{n^0,0}} G_0 \quad (29)$$

(the notation $\{r_k\}$ indicates parametric dependence on the local bath path $(r_0,\ldots,r_N)$) is obtained within the framework of the mapping Hamiltonian using a semiclassical representation of the quantum subsystem propagator. The probability amplitude, $T_{nn^0}(\{r_k\})$, to evolve the quantum subsystem from $|n^0\rangle$ to $|n\rangle$ in a time t, while the local bath follows its path, is described in terms of the evolution of the mapping variable phase space (p_q^t, q^t). This time evolution is determined by propagating a set of initial conditions sampled according to the probability density $G_0 = e^{-\frac{1}{2}\sum_\lambda[(p_{q\lambda}^0)^2+(q_\lambda^0)^2]}$. The classical dynamics of these initial conditions is governed by the Hamiltonian

$$\begin{aligned}h_m(\{r_k\}) = &\frac{1}{2}\sum_\lambda h_{\lambda,\lambda}(\{r_k\})[(p_{q\lambda})^2 + (q_\lambda)^2 - 1] + \frac{1}{2}\\ &\times \sum_{\lambda,\lambda'} h_{\lambda,\lambda'}(\{r_k\})[p_{q\lambda'}p_{q\lambda} + q_{\lambda'}q_\lambda]\end{aligned} \quad (30)$$

In the equation above, the sum runs over all relevant states of the quantum subsystem and $h_{\lambda,\lambda'}(\{r_k\})$ are the matrix elements of the quantum Hamiltonian ($\hat{h}$ in Eq. (1)). Each trajectory contributes to $T_{nn^0}(\{r_k\})$ (see Eq. (29)) through the combination of an amplitude $a_{n,t}(\{r_k\}) = \sqrt{(p_{qn}^t)^2(\{r_k\}) + (q_n^t)^2(\{r_k\})}$, and a phase

$$\begin{aligned}\Theta_{n,t}(\{r_k\}) &= \tan^{-1}\left(\frac{q_n^0}{p_{qn}^0}\right) + \int_0^t d\tau h_{n,n}(r_\tau)\\ &\quad + \int_0^t d\tau \sum_{\lambda\neq n}\left[h_{n,\lambda}(r_\tau)\frac{(q_n^\tau q_\lambda^\tau + p_{qn}^\tau p_{q\lambda}^\tau)}{[(q_n^\tau)^2 + (p_{qn}^\tau)^2]}\right]\\ &= \tan^{-1}\left(\frac{q_n^0}{p_{qn}^0}\right) + \int_0^t \theta_n(r_\tau)d\tau\end{aligned} \quad (31)$$

Both these factors depend parametrically on the local bath evolution, $\{r_k\}$, which at this stage is still expressed at the full quantum level as a path integral. Note also that in the mapping Hamiltonian approach the evolution of the quantum subsystem is obtained from that of an auxiliary dynamical system whose Hamiltonian is quadratic in the mapping variables. Since semiclassical expressions such as the one in Eq. (29) are exact for Hamiltonians of this form, the reduced density matrix element does not contain any approximations other than those employed to evaluate the influence functional. With this exact rewriting, however, the evolution of the quantum subsystem can be implemented using trajectories. On the other hand, as mentioned above, the local bath evolution is still fully quantum and cannot in general be treated exactly.

2.1.4. Linearization, a Langevin Equation, and the fluctuation–dissipation theorem

To obtain a computable result, we now employ a linearized approximation scheme [2,1,5,4,40] to evaluate the path integrals in the expression of the reduced density matrix. Similar to the manipulations of the influence functional above we change variables to the mean, $\bar{r}_k = (r_k + \tilde{r}_k)/2$, and difference, $z_k = r_k - \tilde{r}_k$, local bath coordinates (with similar transformations for the local bath momenta, $\bar{p}_k = (p_k + \tilde{p}_k)/2$ and $y_k = p_k - \tilde{p}_k$). The kinetic action difference term in the phase of the integrand in Eq. (28) is readily written exactly in these mean and difference variables as

$$\begin{aligned}[S(\{r_k\}) - S(\{\tilde{r}_k\})] = &\bar{p}_N z_N - \bar{p}_1 z_0 - \sum_{k=1}^{N-1}(\bar{p}_{k+1} - \bar{p}_k)z_k\\ &- \sum_{k=1}^{N}\left[\frac{\epsilon}{M_b}\bar{p}_k - (\bar{r}_k - \bar{r}_{k-1})\right]y_k\end{aligned} \quad (32)$$

If the counter-term Hamiltonian is considered, the expansion of this part of the action, while no longer purely kinetic, is still

exact and given by $[S_{ct}(\{r_k\}) - S_{ct}(\{\tilde{r}_k\})] = [S(\{r_k\}) - S(\{\tilde{r}_k\})] - \sum_{k=1}^{N}(\sum_J C_J^2/M_B\Omega_J^2)\bar{r}_k z_k \epsilon$, where the sum on J runs over the global bath oscillators. Similarly, Φ_{IF}, in the influence functional can be rewritten in terms of the mean and difference discrete local bath paths yielding:

$$\Phi_{IF} = \epsilon \sum_{k=1}^{N} \left[\alpha_k z_k^2 + i\frac{2\eta}{\pi}(\bar{r}_0 L_k - \Omega_c \bar{r}_k + l_k \bar{p}_k/M_b) z_k \right] \tag{33}$$

Here α_k is the value of the function $\alpha(t)$, defined under Eq. (27), at the kth time slice, with similar definitions for the other time dependent functions.

The central approximation in the linearization approach involves expanding the remaining part of the phase difference $\Theta_{n,t}(\{\bar{r}_k + z_k/2\}) - \tilde{\Theta}_{m,t}(\{\bar{r}_k - z_k/2\})$ in Eq. (28) and truncating this expansion at linear order in the local bath path difference variables, z_k, thus

$$\begin{aligned}&\Theta_{n,t}(\{\bar{r}_k + z_k/2\}) - \tilde{\Theta}_{m,t}(\{\bar{r}_k - z_k/2\}) \\ &= \epsilon \sum_k \left\{ [\theta_n(\bar{r}_k) - \theta_m(\bar{r}_k)] + \frac{1}{2}[\nabla\theta_n(\bar{r}_k) + \nabla\theta_m(\bar{r}_k)] \cdot z_k \right\}\end{aligned} \tag{34}$$

Combining the above results in Eq. (28), the linearized approximation to the reduced density matrix element at time t becomes:

$$\begin{aligned}(\rho_{nm}^{red})_{lin}^{n^0 m^0}(t) = &\int d\bar{r}_0 dz_0 \int \prod_{k=1}^{N} d\bar{r}_k \frac{d\bar{p}_k}{2\pi\hbar} \int \prod_{k=1}^{N} dz_k \frac{dy_k}{2\pi\hbar} \\ &\times \int dp_q^0 dq^0 \int d\tilde{p}_q^0 d\tilde{q}^0 \langle \bar{r}_0 + \frac{z_0}{2}|\hat{\rho}_b|\bar{r}_0 \\ &- \frac{z_0}{2}\rangle e^{-i\bar{p}_1 z_0} \\ &\times a_{n,t}(\{\bar{r}_k\})\tilde{a}_{m,t}(\{\bar{r}_k\}) e^{i\epsilon\sum_{k=1}^{N}\left[\theta_n(\{\bar{r}_k\}) - \tilde{\theta}_m(\{\bar{r}_k\})\right]} e^{-\epsilon\sum_{k=1}^{N}\alpha_k z_k^2} \\ &\times e^{-i\epsilon\sum_{k=1}^{N-1}\left[\frac{(\bar{p}_{k+1}-\bar{p}_k)}{\epsilon} + \frac{\nabla\theta_n(\bar{r}_k)+\nabla\theta_m(\bar{r}_k)}{2} + \frac{2\eta}{\pi}(\bar{r}_0 L_k - \Omega_c\bar{r}_k + l_k\bar{p}_k/M_b)\right] z_k} \\ &\times e^{i\epsilon\sum_{k=1}^{N}\left[\frac{\bar{p}_k}{M} - \frac{(\bar{r}_k - \bar{r}_{k-1})}{\epsilon}\right] y_k} a_{n^0,0}\tilde{a}_{m^0,0} e^{-i(\Theta_{n^0,0} - \tilde{\Theta}_{m^0,0})} G_0 \tilde{G}_0\end{aligned} \tag{35}$$

In the case of the counter-term Hamiltonian, the additional term in the action difference discussed below Eq. (32) is linear in the path difference z_k so can be incorporated into the phase factor term that is linear in z_k in the above Eq. (35) (the second last line). This phase factor for the counter-term Hamiltonian thus takes the form: $e^{-i\chi}$, where

$$\begin{aligned}\chi = \epsilon \sum_{k=1}^{N-1} \Bigg[&\frac{(\bar{p}_{k+1} - \bar{p}_k)}{\epsilon} + \frac{\nabla\theta_n(\bar{r}_k) + \nabla\theta_m(\bar{r}_k)}{2} \\ &+ \sum_J \frac{C_J^2}{M_B\Omega_J^2}\bar{r}_k + \frac{2\eta}{\pi}(\bar{r}_0 L_k - \Omega_c \bar{r}_k + l_k \bar{p}_k/M_b) \Bigg] z_k\end{aligned} \tag{36}$$

Combining the terms in the square brackets that represent forces that are linear in the mean local bath path $\bar{r}_k$ we see they have the form

$$-\frac{2\eta}{\pi}\left(\Omega_c - \frac{\pi}{2\eta}\sum_J \frac{C_J^2}{M_B\Omega_J^2}\right)\bar{r}_k \tag{37}$$

Equating the discrete expression for the spectral density given in Eq. (12) with the exponentially truncated Ohmic form of Eq. (16), and integrating the result over the frequency range $0 \leqslant \Omega \leqslant \infty$ we readily find that

$$\frac{\pi}{2\eta}\sum_J \frac{C_J^2}{M_B\Omega_J^2} = \Omega_c \tag{38}$$

so in the above expression for the linear phase term, the counter-term exactly cancels the divergent linear force that results from the inverted harmonic potential (i.e. $F_{bath}(\bar{r}) = \frac{2\eta}{\pi}\Omega_c\bar{r}$). In the remaining results presented below we will leave out the explicit counter-term consideration as we now know its effect is to simply to cancel the inverted harmonic linear force term.

The linearization approximation makes it possible to perform all integrals over the difference variables, z_k, in Eq. (35) explicitly [2,12]. To proceed we define the Wigner transformed initial local bath density as

$$(\hat{\rho}_b)_W(\bar{r}_0, \bar{p}_1) = \int dz_0 \langle \bar{r}_0 + \frac{z_0}{2}|\hat{\rho}_{b0}|\bar{r}_0 - \frac{z_0}{2}\rangle e^{-i\bar{p}_1 z_0} \tag{39}$$

We use the fact that $\int_{-\infty}^{\infty} dk \exp[ik(x-a)] = 2\pi\delta(x-a)$ and

$$\int_{-\infty}^{\infty} dx e^{-ax^2+bx} = \sqrt{\frac{\pi}{a}} e^{\frac{b^2}{4a}} \tag{40}$$

to evaluate the integrals over the various local bath difference coordinates and momenta in Eq. (35). The result is

$$\begin{aligned}(\rho_{nm}^{red})_{lin}^{n^0 m^0}(t) = &\int d\bar{r}_0 \int \prod_{k=1}^{N} d\bar{r}_k \frac{d\bar{p}_k}{2\pi\hbar} \int dp_q^0 dq^0 \\ &\times \int d\tilde{p}_q^0 d\tilde{q}^0 (\hat{\rho}_b)_W(\bar{r}_0, \bar{p}_1) \\ &\times a_{n,t}(\{\bar{r}_k\})\tilde{a}_{m,t}(\{\bar{r}_k\}) e^{i\epsilon\sum_{k=1}^{N}\left[\theta_n(\{\bar{r}_k\}) - \tilde{\theta}_m(\{\bar{r}_k\})\right]} \\ &\times \prod_{k=1}^{N}\left(\frac{\pi}{\alpha_k\epsilon}\right)^{\frac{1}{2}} e^{-\frac{\epsilon}{4\alpha_k}\left[\frac{(\bar{p}_{k+1}-\bar{p}_k)}{\epsilon} + \frac{\nabla\theta_n(\bar{r}_k)+\nabla\theta_m(\bar{r}_k)}{2} + \frac{2\eta}{\pi}(\bar{r}_0 L_k - \Omega_c\bar{r}_k + l_k\bar{p}_k/M_b)\right]^2} \\ &\times \prod_{k=1}^{N}\delta\left(\frac{\bar{p}_k}{M_b} - \frac{(\bar{r}_k - \bar{r}_{k-1})}{\epsilon}\right) a_{n^0,0}\tilde{a}_{m^0,0} e^{-i(\Theta_{n^0,0} - \tilde{\Theta}_{m^0,0})} G_0 \tilde{G}_0\end{aligned} \tag{41}$$

As described more in detail in the next subsection, the integrals over $\{\bar{r}_k, \bar{p}_k\}$ in the expression above can now be performed and interpreted as a time-stepping algorithm that realizes a stochastic, Brownian-like, dynamics. The delta functions, in fact, specify a fully deterministic evolution for the mean positions of the local bath. The Gaussians, on the other hand, are akin to stochastic propagators in which the values of the momenta at the different times along the mean path are sampled according to a distribution whose mean value is given by the systematic force at that instant plus a frictional dissipative term given by $-2\eta l_k \bar{p}_k/\pi M_b$. In the long time limit, since $\lim_{t'\to\infty} l(t') = \pi/2$, this term reduces to the usual velocity dependent frictional force of the Langevin equation $-\eta p/M_b$.

As required by the fluctuation–dissipation theorem, the dissipative term described above must be accompanied by a random fluctuating force contribution, and the properties of the random fluctuating force distribution must be related in the usual way to the characteristics of the frictional force. This important feature arises in the approach outlined above from the stochastic Gaussian propagator term appearing in Eq. (41). As summarized in the next section, the algorithm we have developed for implementing Eq. (41), involves sampling a Gaussian distributed random number, ξ, at each step, and equating it to the term that is squared in the argument of the Gaussian in that equation. The result of this equality can be written in the form of a stochastic differential equation as follows:

$$\begin{aligned}\frac{d\bar{p}}{dt} = &-\frac{1}{2}[\nabla\theta_n(\bar{r}(t)) + \nabla\theta_m(\bar{r}(t))] - \frac{2\eta}{\pi}[\bar{r}(0)L(t) - \Omega_c\bar{r}(t) \\ &+ l(t)\bar{p}(t)/M_b] + \xi(t)\end{aligned} \tag{42}$$

From Eq. (41) we see that when we increment the solution by a discrete time step, the standard deviation of the distribution of fluctuations in the random force during the kth step of duration ϵ is $\sigma_{\xi_k}^2 = 2\alpha_k/\epsilon$. Let the random fluctuation of the force at time t from its mean value be $\delta F(t) = F(t) - \langle F\rangle$. Then the usual form of

the fluctuation–dissipation theorem states that the random fluctuating force is uncorrelated on sufficiently long time-scales compared to the typical fast relaxation times, and that the magnitude of its correlation function is related to the friction constant, η, and the inverse temperature, $\beta = 1/k_B T$, according to the following classical result:

$$\langle \delta F(t)\delta F(0)\rangle = \frac{2\eta}{\beta}\delta(t) \tag{43}$$

Integrating this expression on the range $-\epsilon/2 \leqslant t \leqslant \epsilon/2$ and assuming that the correlation function is constant at its zero time value over this time interval, we can write the integrated form of this result as $\langle \delta^2 F(0)\rangle \epsilon = 2\eta/\beta$. Substituting for the standard deviation of the random fluctuating force obtained above from Eq. (41) we find that the fluctuation–dissipation theorem requires that $\alpha_k = \eta/\beta$. Recalling the result under Eq. (27) we have

$$\alpha_k = \alpha(t_k) = \int_0^{t_k} d\tau \alpha_R(\tau) \tag{44}$$

Taking the high temperature limit of Eq. (18) we readily find (with $\hbar = 1$) that

$$\lim_{\beta\to 0} \alpha_R(\tau) = \frac{2\eta}{\pi\beta}\frac{\Omega_c}{[1+(\Omega_c\tau)^2]} \tag{45}$$

Thus, since $\int_0^\infty d\tau \Omega_c/[1+(\Omega_c\tau)^2] = \pi/2$, we see that the fluctuation–dissipation theorem result is recovered when we take the long time limit of the integral as $\alpha_\infty = \eta/\beta$.

Before describing the evolution scheme that corresponds to the above combination of Green functions, however, let us further analyze the linearization approximation. There are three contributing factors that can keep the z_k deviations small and make the linearization approximation reliable: (1) If the total propagation time, t, is short the forward and backward paths must remain close to one another as there is insufficient time for them to evolve in significantly different ways. Generally, as the propagation time becomes longer the deviations between forward and backward paths can grow resulting in linearization providing a poorer approximation for long time evolution. (2) In a condensed phase environment, like that modeled by the harmonic global bath used in the above developments, the real exponential part of the influence functional contribution results in the gaussian form in the forward-backward local bath path difference, i.e. the term $\exp[-\epsilon\sum_{k=1}^N \alpha_k z_k^2]$ appearing in Eq. (35). As discussed earlier, see Eq. (18), α_k depends linearly on the friction appearing in the coupling between the local and global baths. If the global environmental friction, η, is strong making α_k large, the gaussian term will limit the size of the fluctuations in z_k, thus improving the reliability of the linearization approximation. (3) Finally, $\alpha(t)$ also becomes large with increasing temperature so the linearization approximation should improve in this limit. The numerical results presented in Section 3 explore the interplay of these various contributing effects on the reliability of the linearization approximation for a spin-boson (system-local bath) model.

2.2. A mixed quantum-classical Brownian dynamics approach

The approximate form of the density matrix dynamics developed in Eq. (41) can be implemented using a stochastic Brownian dynamics procedure that we summarize as follows:

1. Initial and final quantum subsystem density matrix state labels ($|n^0\rangle|m^0\rangle$, and $|n\rangle|m\rangle$ respectively) are selected and initial values of the mapping variables are assigned accordingly. We use the "focusing" approach for this purpose which amounts to performing the integrations over initial mapping variables using a steepest descent approximation (see reference [41] for details).
2. Initial values of the local bath positions and momenta $(\bar r_0, \bar p_1)$ are sampled from the Wigner transformed initial distribution $(\hat\rho_b)_W(\bar r_0, \bar p_1)$. This sampling performs the $\bar r_0, \bar p_1$ integrals by a Monte Carlo procedure.
3. Next, the integral over $d\bar r_1$ is performed, determining $\bar r_1$ from the argument of the δ-function as
$$\bar r_1 = \bar r_0 + \epsilon\frac{\bar p_1}{M_b}$$
4. The mapping variables can be advanced to the next step using $\bar r_1$ to compute the matrix elements in Eq. (30). This provides all the necessary information to compute new values of the functions $\theta_n(\bar r_1)$ that are used in the mapping Hamiltonian and defines the mapping variable equations of motion.
5. Now all the quantities necessary to specify the new time step's gaussian momentum distribution, $\exp[-\frac{1}{4\alpha_2\epsilon}(\bar p_2 - \bar p_2^*)^2]$, are available. Here
$$\bar p_2^* = \bar p_1 - \epsilon\left[\frac{\nabla\theta_n(\bar r_1) + \nabla\theta_m(\bar r_1)}{2} + \frac{2\eta}{\pi}\left(\bar r_0 L_1 - \Omega_c \bar r_1 + l_1\frac{\bar p_1}{M_b}\right)\right] \tag{46}$$
is the center of the new gaussian momentum distribution. It is determined by a force term arising from the gradients of the functions θ_n and θ_m, a time dependent force, $2\eta\bar r_0\frac{L_1}{\pi}$, an inverted harmonic force term, $\frac{-2\eta\Omega_c}{\pi}\bar r_1$, coming from the interaction between the local and global bath degrees of freedom (this term is cancelled in the counter-term Hamiltonian), and finally a frictional dissipative term, $\frac{2\eta l_1}{\pi M_b}\bar p_1$, in which the force depends on the current velocity and the strength of the friction η arising from the coupling to the global bath. As discussed above, in accord with the fluctuation–dissipation theorem, this dissipative term is accompanied by gaussian momentum fluctuations that are incorporated by sampling $\bar p_2$ values from this shifted gaussian distribution. Thus the integral over $\bar p_2$ is performed by a direct gaussian sampling procedure. The width of the distribution of momentum fluctuations in this Brownian dynamics scheme is $\sigma_2 = \sqrt{2\alpha_2\epsilon}$. We compute α_2 by numerical integration (see Eq. (18), and the definition after Eq. (27)).
6. The sampled value of $\bar p_2$ determines $\bar r_2$ according to the next δ-distribution when the cycle repeats starting at step (3).

The approach outlined above employs the linearization approximation for the entire propagation. In this respect it is similar to the earlier LANDmap approach we developed, and is detailed in reference [6]. In LANDmap the evolution of all degrees of freedom is treated explicitly and linearization of the path integrals for the local and global bath variables results in a deterministic dynamics in contrast to the stochastic approach we develop here in which the global bath degrees of freedom are integrated out. A comparison between the performance of these approaches will be presented in the results section. The linearized dynamics can be used iteratively as a short time approximation to improve the accuracy of this approach for longer time propagation (this is the ISLAND-map algorithm [15]). An analogous iterative procedure can be developed for the stochastic approach outlined above. In this iterative scheme many short time propagation segments represented by Eq. (41) are concatenated. Thus, for example, the reduced density matrix at time $2t$ is obtained as:

$$
\begin{aligned}
(\rho^{red}_{n^{2t}m^{2t}})^{n^0m^0}_{lin}(2t) = & \int \prod_{k=N}^{2N} d\bar{r}_k \frac{d\bar{p}_k}{2\pi\hbar} a_{n^{2t},2t}(\{\bar{r}_k\}) \tilde{a}_{m^{2t},2t}(\{\bar{r}_k\}) \\
& \times e^{i\epsilon \sum_{k=N+1}^{2N} \left[\theta_{n^{2t}}(\{\bar{r}_k\}) - \tilde{\theta}_{m^{2t}}(\{\bar{r}_k\})\right]} \times \prod_{k=N+1}^{2N} \left(\frac{\pi}{\alpha_k \epsilon}\right)^{\frac{1}{2}} \\
& \times e^{-\frac{\epsilon}{4\alpha_k}\left[\frac{(\bar{p}_{k+1}-\bar{p}_k)}{\epsilon} + \frac{\nabla^\theta_{n^{2t}}(\bar{r}_k) + \nabla^\theta_{m^{2t}}(\bar{r}_k)}{2} + \frac{2\eta}{\pi}(\bar{r}_N L_k - \Omega_c \bar{r}_k + l_k \bar{p}_k/M_b)\right]^2} \\
& \times \prod_{k=N+1}^{2N} \delta\left(\frac{\bar{p}_k}{M_b} - \frac{(\bar{r}_k - \bar{r}_{k-1})}{\epsilon}\right) \times \sum_{n^t,m^t} \int dp^t_q dq^t \\
& \times \int d\tilde{p}^t_q d\tilde{q}^t a_{n^t,t} \tilde{a}_{m^t,t} e^{-i(\Theta_{n^t,t} - \tilde{\Theta}_{m^t,t})} G_t \widetilde{G}_t \\
& \times \delta(\bar{p}_N - \bar{p}_{N+1}) \delta\left(\frac{\bar{p}_N}{M_b} - \frac{(\bar{r}_N - \bar{r}_{N-1})}{\epsilon}\right) \\
& \times \int d\bar{r}_0 \int \prod_{k=1}^{N-1} d\bar{r}_k \frac{d\bar{p}_k}{2\pi\hbar} a_{n^t,t}(\{\bar{r}_k\}) \tilde{a}_{m^t,t}(\{\bar{r}_k\}) \\
& \times e^{i\epsilon \sum_{k=1}^{N} \left[\theta_{n^t}(\{\bar{r}_k\}) - \tilde{\theta}_{m^t}(\{\bar{r}_k\})\right]} \times \prod_{k=1}^{N} \left(\frac{\pi}{\alpha_k \epsilon}\right)^{\frac{1}{2}} \\
& \times e^{-\frac{\epsilon}{4\alpha_k}\left[\frac{(\bar{p}_{k+1}-\bar{p}_k)}{\epsilon} + \frac{\nabla^\theta_{n^t}(\bar{r}_k) + \nabla^\theta_{m^t}(\bar{r}_k)}{2} + \frac{2\eta}{\pi}(\bar{r}_0 L_k - \Omega_c \bar{r}_k + l_k \bar{p}_k/M_b)\right]^2} \\
& \times \prod_{k=1}^{N-1} \delta\left(\frac{\bar{p}_k}{M_b} - \frac{(\bar{r}_k - \bar{r}_{k-1})}{\epsilon}\right) \times \int dp^0_q dq^0 \\
& \times \int d\tilde{p}^0_q d\tilde{q}^0 a_{n^0,0} \tilde{a}_{m^0,0} e^{-i(\Theta_{n^0,0} - \tilde{\Theta}_{m^0,0})} G_0 \widetilde{G}_0 (\hat{\rho}_b)_W(\bar{r}_0, \bar{p}_1)
\end{aligned}
\tag{47}
$$

In constructing the Brownian dynamics propagator we have assumed that the global bath is initially in thermal equilibrium enabling us to integrate out these variables and include their effects on the local bath dynamics in terms of the dynamically non-local influence functional. The same assumption has been implicitly made for the density matrix at the beginning of each time segment to obtain the above iterative scheme. This assumption should not hold in general, however, we will show in model studies reported below that reasonable results can often be obtained. In future work we will explore the conditions under which this approach provides a good approximation, and develop means to correct for energy dissipation to the global bath that is not accounted for correctly in the current scheme.

3. Results

3.1. Spin-Boson Local bath coupled to independent boson global bath

The goal of the model calculations we describe below is two-fold: First we will explore how the linearized propagator becomes accurate for longer times in a condensed phase environment as a function of the critical environmental parameters identified in the theoretical analysis namely η, Ω_c, and β. Here the focus will be on comparing fully linearized approximate results with converged ISLAND-map calculations. This multi-state iterative density matrix propagation scheme should provide exact results in the limit of many iterations. Second, we will assess the performance of the stochastic scheme derived in this paper by comparing the results of the iterative Brownian dynamics approach that integrates out the global bath variables analytically, with results from full dimensional ISLAND-map calculations.

The form of our model Hamiltonian is

$$
\widehat{H} = \widehat{H}_{s-b} + \widehat{H}_{b-B} \tag{48}
$$

where the quantum system-local bath Hamiltonian, $\widehat{H}_{s-b}$ is the standard symmetric spin-boson form

$$
\widehat{H}_{s-b} = \sum_{j=1}^{m} \frac{1}{2}(p_j^2 + \omega_j^2 r_j^2)\hat{\mathbf{1}} + \sum_{j=1}^{m} c_j r_j \hat{\sigma}_z + \Delta\hat{\sigma}_x \tag{49}
$$

A simple model system to which we can readily apply the influence functional approach outlined in Section 2 involves coupling each local bath oscillator to its own independent global bath. In this case the local bath-global bath Hamiltonian has the form:

$$
\widehat{H}^{ind}_{b-B} = \left[\sum_{j=1}^{m}\sum_{J=1}^{M} \frac{1}{2}(P_J^{(j)^2} + \Omega_J^{(j)^2} R_J^{(j)^2}) + C_J^{(j)} R_J^{(j)} r_j\right]\hat{\mathbf{1}} \tag{50}
$$

As discussed in the Theory section and shown below, this model Hamiltonian, with bilinear coupling between the local and global baths, exhibits some curious behavior in the limit of strong coupling [27,24]. The "counter-term" modified Hamiltonian corresponding to the model above takes the form:

$$
\begin{aligned}
\widehat{H}^{ind}_{b-B} &= \left[\sum_{j=1}^{m}\sum_{J=1}^{M} \frac{1}{2}(P_J^{(j)^2} + \Omega_J^{(j)^2} R_J^{(j)^2}) + C_J^{(j)} R_J^{(j)} r_j + \frac{C_J^{(j)^2}}{2\Omega_J^{(j)^2}} r_j^2\right]\hat{\mathbf{1}} \\
&= \left[\sum_{j=1}^{m}\sum_{J=1}^{M} \frac{1}{2}P_J^{(j)^2} + \frac{1}{2}\Omega_J^{(j)^2}(R_J^{(j)} + \frac{C_J^{(j)}}{\Omega_J^{(j)^2}} r_j)^2\right]\hat{\mathbf{1}}
\end{aligned}
\tag{51}
$$

In the following we will present results both for the "standard" and the counter-term modified Hamiltonian.

For convenience we choose each of the independent global bath-local bath oscillator spectral densities to be identical, though this simplification is unnecessary. Thus, in our calculations, the $C_J^{(j)}$ and $\Omega_J^{(j)}$ are sampled from the smooth, exponential cutoff Ohmic spectral density, $J(\Omega) = \eta\Omega \exp[-\Omega/\Omega_c]$, for a global bath medium with damping constant η.

The quantum system-local bath coupling constants, c_j, and local bath frequencies, ω_j, are determined by a similar exponential cutoff Ohmic spectral density, $J^{loc}(\omega) = \eta^{loc}\omega \exp[-\omega/\omega_c]$, with different damping constant η^{loc}, and cutoff frequency ω_c. In the studies presented below these parameters were assigned the following values: $\eta^{loc} = 0.5, \omega_c = 1.0$. The off-diagonal coupling in the spin-boson Hamiltonian was $\Delta = 0.333$. In all the figures below various quantities are plotted as functions of reduced time, $\tau = t\Delta$.

The model studies presented below explore the general prediction of the influence functional theory arguments made in Section 2 which suggest that the reliability of the linearization approximation for longer times in condensed phase applications depends on the coupling between the local and global baths controlled by η, and the temperature. The approximation that enables simplification of the multiple time integrals using the strongly peaked nature of the kernels, α_R, and α_I, will also be explored by varying the cutoff frequency Ω_c. As these quantities increase linearization becomes accurate for longer times. This will be tested by comparing linearized results with those obtained using the full dimensional iterative scheme that provides a benchmark. We will also explore the reliability of the Brownian dynamics scheme introduced in the previous section and its approximate iterative implementation.

In Fig. 2 (see caption for details) we explore the influence of global bath cutoff frequency Ω_c, and temperature for a fixed small value of global bath friction $\eta = 0.05$. The results compared are for the standard Hamiltonian (not including the counter-term). The general trend observed is that the linearized approximation becomes more accurate with increasing values of Ω_c. This improvement is more pronounced at higher temperatures. Both these observations are consistent with the theoretical analysis presented in Section 2.1. The figure also demonstrates the good agreement between the iterative scheme Brownian dynamics results and converged ISLAND-map calculations. Generally the linearized Brownian results agree well with linearized full system dynamical

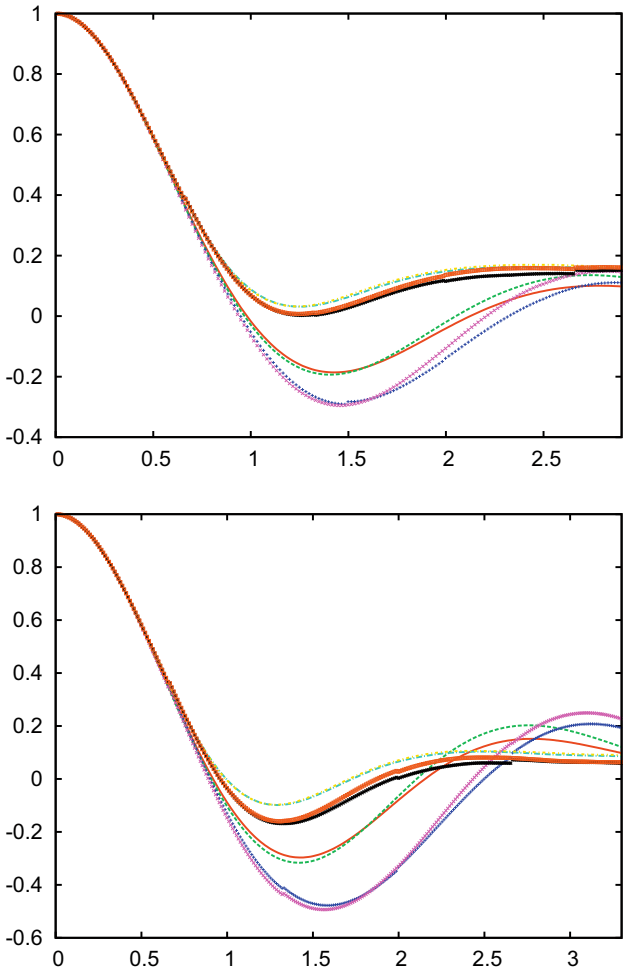

Fig. 2. Spin state population difference, $\langle\sigma_z\rangle(\tau)$, for $\eta^{loc} = 0.5, \eta = 0.05$. There are 20 local bath oscillators whose frequencies are sampled from an exponential distribution. Each local bath oscillator is coupled to its own independent set of 20 global bath oscillators. In each panel there are two sets of four curves. The "lower" set of curves corresponds to spectral densities characterized by local and global bath cutoff frequencies $\omega_c = 1.0$ and $\Omega_c = 1.0$, respectively. The "upper" set of curves in each panel has cutoff frequencies $\omega_c = 1.0$ and $\Omega_c = 10.0$. The top panel corresponds to moderate temperature $\beta = 3.0$, and the bottom panel presents low temperature results with $\beta = 12.5$. The different color and dash pattern curves show results obtained with different methods. The "lower" set of curves ($\Omega_c = 1.0$) is: LANDmap = solid red curve; Brownian = green dashed curve; ISLAND-map (5 iterations) = blue crosses; ISBrownian (5 iterations) = magenta x's. The "upper" set of curves ($\Omega_c = 10.0$) is: LANDmap = long dash-dot light blue curve; Brownian = dash-dot yellow curve; ISLAND-map (5 iterations) = black symbols; ISBrownian (5 iterations) = orange symbols. (For interpretation of the references to colour in this figure legend, the reader is referred to the web version of this article.)

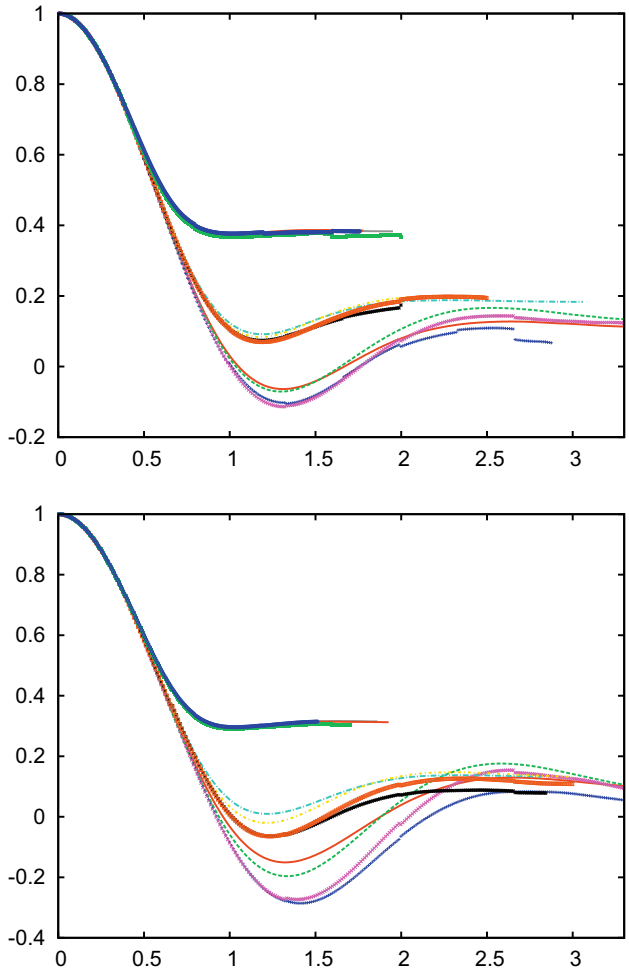

Fig. 3. Spin state population difference, $\langle\sigma_z\rangle(\tau)$, for $\eta^{loc} = 0.5, \eta = 0.5$. The numbers of oscillators are the same as for Fig. 2. In each panel there are three sets of four curves. Top panel has $\beta = 3.0$, and bottom panel has $\beta = 12.5$. The "lower" and "middle" sets of curves have $\Omega_c = 1.0$ and $\Omega_c = 2.0$ respectively and the same color scheme as in Fig. 2. The "top" set of curves has $\Omega_c = 5.0$ where all methods give results that are essentially superimposable.

results, and the same is true when the iterative algorithm is employed though differences appear at longer times.

The results presented in Fig. 3 extend the analysis to larger values of global bath friction ($\eta = 0.5$), and for a range of cutoff frequencies (Ω_c =1.0, 2.0, and 5.0). The trends observed for smaller friction are confirmed: linearization becomes even more accurate both at high and low temperature with increasing Ω_c, and the Brownian dynamics scheme is again seen to give reliable results. For this strong global bath friction limit, however, we observe that the spin population difference does not equilibrate to zero. This behavior is unphysical since the model we are studying is a symmetric spin-boson (the two diabatic state energies are degenerate so at thermal equilibrium the populations should be the same). This occurs because of the nature of the coupling between the local and global baths in the standard model Hamiltonian used in these calculations, and arises from evolving the non-equilibrium initial conditions used in studies with this Hamiltonian, in the strong friction limit. Analogous unphysical behavior has been discussed at length in the literature [27]. When the global bath friction, and therefore the couplings $C_j^{(j)}$, are sufficiently large, the bilinear coupling term in Eq. (50) dominates the dynamics of the local bath variables which becomes unbounded. The off-diagonal term in the spin-boson Hamiltonian ($\Delta\hat{\sigma}_x$) also becomes negligible compared to this unbounded term, and population equilibration is compromised. The counter-term modified Hamiltonian in Eq. (51) gives bounded dynamics and thus avoids these problems.

The effect of the counter-term is demonstrated in Fig. 4 where we present results for both diagonal (populations) and off-diagonal density matrix elements (coherences). In the left panel, in the absence of the counter-term, the unstable local bath dynamics results in rapid decay of the coherence elements and the population difference does not equilibrate for strong global bath friction. The results presented in the center and right panels are obtained with the same global bath parameters but now, with the counter-term modified Hamiltonian, the stable local bath dynamics gives long lived coherences and the populations can relax to equilibrium. From

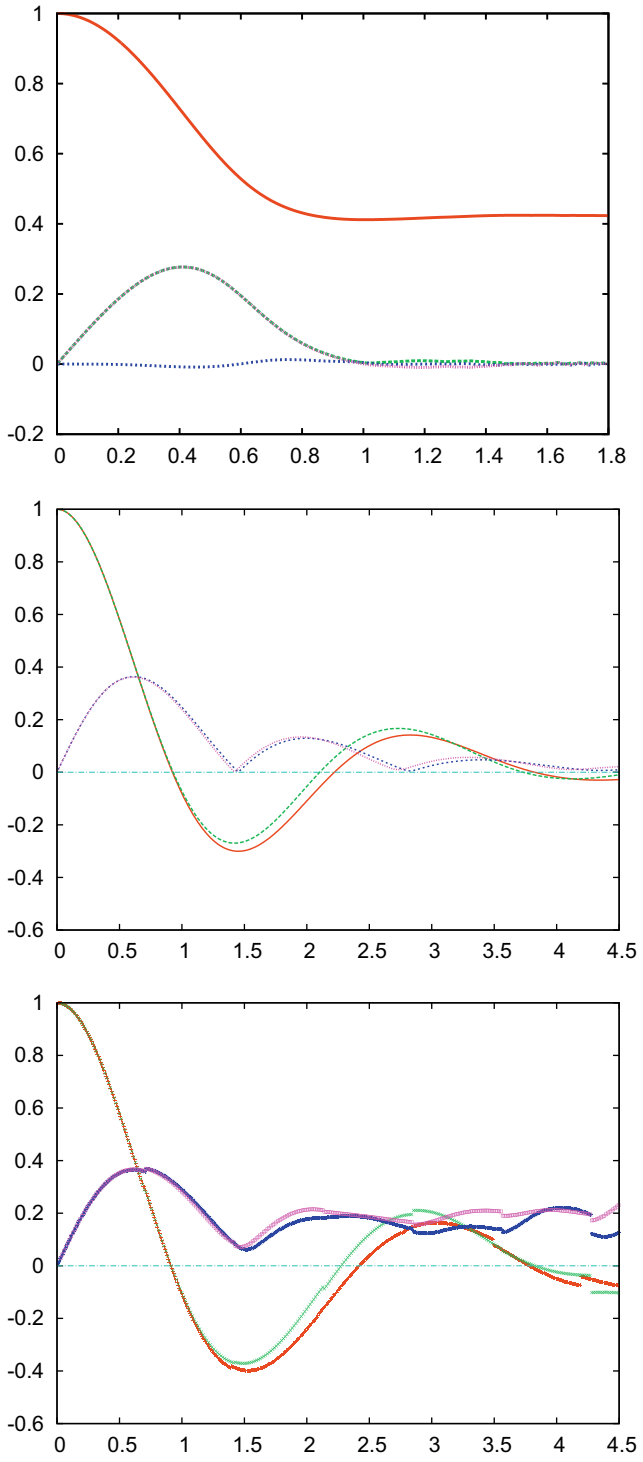

Fig. 4. Spin state population difference, $\rho_{11}(\tau) - \rho_{22}(\tau) = \langle \sigma_z \rangle(\tau)$, and density matrix coherence elements $\rho_{12}(\tau)$, for $\eta^{loc} = 0.5, \omega_c = 1, \eta = 0.5, \Omega_c = 5.0, \beta = 3.0$. Top Panel: no counter-term (all methods give identical results), solid red curve is $\langle \sigma_z \rangle(\tau)$, green dashed curve is $|\rho_{12}|(\tau)$, magenta curve is $\mathrm{Re}[\rho_{12}](\tau)$, blue dots $\mathrm{Im}[\rho_{12}](\tau)$. Center panel: counter-term included, red and green curves show $\langle \sigma_z \rangle(\tau)$, for the full linearized and linearized Brownian algorithms respectively. Blue and magenta curves present $|\rho_{12}|(\tau)$ for these methods. Bottom panel presents results for iterative linearized and iterative Brownian dynamics (10 iterations), same color scheme as center panel. (For interpretation of the references to colour in this figure legend, the reader is referred to the web version of this article.)

the right hand panel we see that the iterative scheme gives a more accurate account of this long lived coherent dynamics.

4. Conclusion

In this paper we explore how the linearized approximation becomes accurate for a model condensed phase system, composed of a quantum subsystem coupled to a local environment which in turn is coupled to a global bath. The results presented in Section 3 support the theoretical analysis given in Section 2 and confirm that linearization is accurate for the long time dynamics of this system when the coupling between the local and global environments is strong, and the global bath has a broad frequency distribution.

We have also introduced a new linearized stochastic density matrix propagation algorithm. We explored the properties of this approach and demonstrated that it satisfies the fluctuation–dissipation theorem in various limits. Results of calculations using this new approach are essentially as accurate as those obtained with the full system linearized propagation approach. In the new scheme, however, the global bath degrees of freedom are integrated out and the reduction of the number of degrees of freedom that must be evolved explicitly provides a potential advantage with this approach. The accuracy of the approach for longer times can be improved using an iterative implementation. This implementation contains an additional approximation: it assumes a "product form" density matrix in which the global bath is in thermal equilibrium, at a fixed temperature, at the beginning of each iteration. Our results provide numerical evidence suggesting that these approximations, that appear reasonable in the weak coupling limit, can be reliable even for moderate to strong local bath-global bath coupling. Future work will focus on further exploring theoretically and numerically the origins and reliability of these observations.

Systematic procedures for partitioning the bath into its constituent local and global components that influence the short time dynamics, and longer time dissipative effects, respectively, have been discussed [22,23]. With hierarchical approaches that make assumptions about separations of time-scales often one must absorb the local bath degrees of freedom into the definition of the quantum subsystem due of the fast timescale on which these degrees of freedom evolve. This added complication may not be necessary with the linearized dynamics procedure described in this paper and it will be useful to compare our approach with other hierarchical methods that require this separation of time-scales.

Acknowledgements

We gratefully acknowledge support for this research from the National Science Foundation under Grant CHE-0616952, and CHE-0911635, and funding from the Italian Ministero dell' Ambiente e della Tutela del Territorio e del Mare. DFC acknowledges the support of his Stokes Professorship in Nanobiophysics from Science Foundation Ireland.

References

[1] R. Hernandez, G. Voth, Quantum time correlation functions and classical coherence, Chem. Phys. 223 (1998) 243.
[2] J. Poulsen, G. Nyman, P. Rossky, Practical evaluation of condensed phase quantum correlation functions: a Feynman–Kleinert variational linearized path integral method, J. Chem. Phys. 119 (2003) 12179.
[3] J. Poulsen, G. Nyman, Determination of the Van Hove spectrum of liquid He(4): an application of the Feynman–Kleinert linearized path integral methodology, J. Phys. Chem. A 108 (2004) 8743.
[4] Q. Shi, E. Geva, Semiclassical theory of vibrational energy relaxation in the condensed phase, J. Phys. Chem. A 107 (2003) 9059.
[5] Q. Shi, E. Geva, A relationship between semiclassical and centroid correlation functions, J. Chem. Phys. 118 (2003) 8173.
[6] S. Bonella, D.F. Coker, Land-map, a linearized approach to nonadiabatic dynamics using the mapping formalism, J. Chem. Phys. 122 (2005) 194102.
[7] S. Bonella, D. Montemayor, D.F. Coker, Linearized path integral approach for calculating nonadiabatic time correlation functions, Proc. Natl. Acad. Sci. 102 (2005) 6715.

[8] D.F. Coker, S. Bonella, Linearized path integral methods for quantum time correlation functions, in: M. Ferrario, G. Ciccotti, K. Binder (Eds.), Computer Simulations in Condensed Matter: From Materials to Chemical Biology, Lecture Notes in Physics, vol. 703, Springer-Verlag, Berlin, 2006, p. 553.
[9] J. Poulsen, G. Nyman, P. Rossky, Static and dynamic quantum effects in molecular liquids: a linearized path integral description of water, Proc. Nat. Acad. Sci. 102 (2005) 6709.
[10] Q. Shi, E. Geva, On the calculation of vibrational energy relaxation rate constants from centroid molecular dynamics simulations, J. Chem. Phys. 119 (2003) 9030.
[11] Q. Shi, E. Geva, Vibrational energy relaxation rate constants from linear response theory, J. Chem. Phys. 118 (2003) 7562.
[12] S. Causo, G. Ciccotti, D. Montemayor, S. Bonella, D. Coker, An adiabatic linearized path integral approach for quantum time correlation functions: electronic transport in metal-molten salt solutions, J. Phys. Chem. B 109 (2005) 6855.
[13] Z. Ma, D. Coker, Quantum initial condition sampling for linearized density matrix dynamics: vibrational pure dephasing of iodine in krypton matrices, J. Chem. Phys. 128 (2008) 244108.
[14] S. Bonella, G. Ciccotti, R. Kapral, Linearization approximations and Liouville quantum-classical dynamics, Chem. Phys. Letts. 484 (2010) 399.
[15] E. Dunkel, S. Bonella, D. Coker, Iterative linearized approach to non-adiabatic dynamics, J. Chem. Phys. 129 (2008) 114106.
[16] R. Kapral, G. Ciccotti, Mixed quantum-classical dynamics, J. Chem. Phys. 110 (1999) 8919.
[17] S. Nielsen, R. Kapral, G. Ciccotti, Mixed quantum-classical surface hopping dynamics, J. Chem. Phys. 112 (2000) 6543.
[18] D. Mackernan, G. Ciccotti, R. Kapral, Trotter-based simulation of quantum-classical dynamics, J. Phys. Chem. B 112 (2008) 424.
[19] A. Garg, J. Onuchic, V. Ambergaokar, J. Chem. Phys. 83 (1985) 4491.
[20] Y. Tanimura, S. Mukamel, J. Phys. Soc. Jpn. 63 (1994) 66.
[21] S. Mukamel, Principles of Nonlinear Optical Spectroscopy, Oxford University Press, New York, 1995.
[22] K. Hughes, C. Christ, I. Burghardt, J. Chem. Phys. 131 (2009) 024109.
[23] K. Hughes, C. Christ, I. Burghardt, J. Chem. Phys. 131 (2009) 124108.
[24] K. Shiokawa, R. Kapral, Emergence of quantum-classical dynamics in an open quantum environment, J. Chem. Phys. 117 (2002) 7852.
[25] R. Feynman, F. Vernon, Ann. Phys. N.Y. 24 (1963) 118.
[26] A. Caldeira, A. Leggett, Path integral approach to quantum Brownian motion, Physica 121A (1983) 587.
[27] U. Weiss, Quantum Dissipative Systems, second ed., World Scientific, Singapore, 1999.
[28] M. Topaler, N. Makri, Quantum rates for a double well coupled to a dissipative bath: accurate path integral results and comparison with approximate theories, J. Chem. Phys. 101 (1994) 7500.
[29] S. Zhang, E. Pollak, J. Chem. Phys. 118 (2003) 4357.
[30] E. Pollak, J. Chem. Phys. 127 (2007) 074505.
[31] J. Moix, E. Pollak, J. Chem. Phys. 129 (2008) 064515.
[32] Q. Shi, E. Geva, A derivation of the mixed quantum-classical Liouville equation from the influence functional formalism, J. Chem. Phys. 121 (2004) 3393.
[33] E. Pollak, J. Shao, D. Zhang, Phys. Rev. E 77 (2008) 021107.
[34] H. Kleinert, Path Integrals in Quantum Mechanics, Statics, Polymer Physics and Financial Markets, World Scientific, Singapore, 2004.
[35] P. Huo, S. Bonella, D.F. Coker, Local bath-global bath models with quantum subsystem state dependent friction, in preparation.
[36] W. Miller, C. McCurdy, Classical trajectory model for electronically nonadiabatic collision phenomena. A classical analog for electronic degrees of freedom, J. Chem. Phys. 69 (1978) 5163.
[37] G. Stock, M. Thoss, Semiclassical description of nonadiabatic quantum dynamics, Phys. Rev. Lett. 78 (1997) 578.
[38] M. Thoss, G. Stock, Mapping approach to the semiclassical description of nonadiabatic quantum dynamics, Phys. Rev. A 59 (1999) 64.
[39] X. Sun, W. Miller, Semiclassical initial value representation for electronically nonadaibatic molecular dynamics, J. Chem. Phys. 106 (1997) 6346.
[40] Q. Shi, E. Geva, Vibrational energy relaxation in liquid oxygen from a semiclassical molecular dynamics simulation, J. Phys. Chem. A 107 (2003) 9070.
[41] S. Bonella, D.F. Coker, Semi-classical implementation of the mapping Hamiltonian approach for non-adiabatic dynamics: focused initial distribution sampling, J. Chem. Phys. 118 (2003) 4370.